Acta Crystallographica Section F
Structural Biology and Crystallization Communications
ISSN 1744-3091

New crystal structure of the proteasome-dedicated chaperone Rpn14 at 1.6 Å resolution

Sangwoo Kim,[a] Akira Nishide,[b] Yasushi Saeki,[c] Kenji Takagi,[b] Keiji Tanaka,[c] Koichi Kato[a,d] and Tsunehiro Mizushima[b]*

[a]Graduate School of Pharmaceutical Sciences, Nagoya City University, 3-1 Tanabe-dori, Mizuho-ku, Nagoya 467-8603, Japan, [b]Picobiology Institute, Department of Life Science, Graduate School of Life Science, University of Hyogo, 3-2-1 Kouto, Kamigori-cho, Ako-gun, Hyogo 678-1297, Japan, [c]Laboratory of Protein Metabolism, Tokyo Metropolitan Institute of Medical Science, 2-1-6 Kamikitazawa, Setagaya-ku, Tokyo 156-8506, Japan, and [d]Institute for Molecular Science and Okazaki Institute for Integrative Bioscience, National Institutes of Natural Sciences, 5-1 Higashiyama, Myodaiji, Okazaki 444-8787, Japan

Correspondence e-mail: mizushi@sci.u-hyogo.ac.jp

Received 15 February 2012
Accepted 15 March 2012

PDB Reference: yeast Rpn14 E384A mutant, 3vl1.

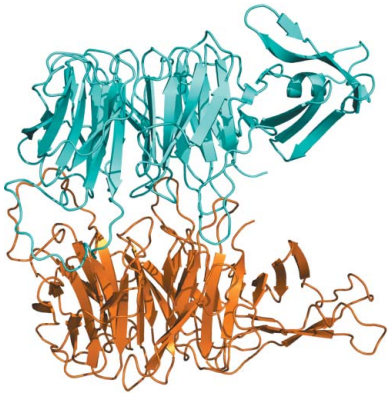

The 26S proteasome is an ATP-dependent protease responsible for selective degradation of polyubiquitylated proteins. Recent studies have suggested that proteasome assembly is a highly ordered multi-step process assisted by specific chaperones. Rpn14, an assembly chaperone for ATPase-ring formation, specifically recognizes the ATPase subunit Rpt6. The structure of Rpn14 at 2.0 Å resolution in space group $P6_4$ has previously been reported, but the detailed mechanism of Rpn14 function remains unclear. Here, a new crystal structure of Rpn14 with an E384A mutation is presented in space group $P2_1$ at 1.6 Å resolution. This high-resolution structure provides a framework for understanding proteasome assembly.

1. Introduction

The 26S proteasome is a highly conserved protein-degradation machine that regulates a variety of cellular processes by the selective breakdown of short-lived and abnormal proteins in eukaryotes (Finley, 2009; Tanaka, 2009). This proteasome comprises a catalytic 20S core particle (CP) and 19S regulatory particles (RPs). The 19S RPs recognize polyubiquitylated substrate proteins and take part in their deubiquitination, unfolding and translocation into the interior of the CP for destruction. The RP comprises base and lid subcomplexes. The base is composed of six different homologous AAA+ ATPase subunits (Rpt1–Rpt6) and three additional non-ATPase subunits (Rpn1, Rpn2 and Rpn13), whereas the lid is composed of at least nine non-ATPase subunits. Identification of the CP-dedicated chaperones, such as hUmp1/Ump1, PAC1/Pba1/Poc1, PAC2/Pba2/Poc2, PAC3/Pba3/Poc3/Dmp2 and PAC4/Pba4/Poc4/Dmp1, revealed that proteasome biogenesis is a highly ordered multi-step event rather than a simple self-assembly (Murata *et al.*, 2009; Ramos & Dohmen, 2008; Rosenzweig & Glickman, 2008). Recently, four chaperones that contribute to assembly of the 19S RP base (Nas2/p27, Nas6/gankyrin, Rpn14/PAAF1 and Hsm3/S5b) have been identified (Funakoshi *et al.*, 2009; Saeki *et al.*, 2009; Roelofs *et al.*, 2009; Le Tallec *et al.*, 2009; Kaneko *et al.*, 2009; Tomko *et al.*, 2010; Sakata *et al.*, 2011). It has been proposed that each of these factors associates with a specific base ATPase subunit and assists in formation of the ATPase ring in the 19S RP. Rpn14 specifically binds the C-terminal domain of Rpt6 to form a tetrameric assembly intermediate, Nas6–Rpt3–Rpt6–Rpn14, during ATPase-ring formation (Funakoshi *et al.*, 2009; Saeki *et al.*, 2009).

We have previously reported the X-ray crystal structure of wild-type yeast Rpn14 in space group $P6_4$ containing one molecule in the asymmetric unit at 2.0 Å resolution (Kim *et al.*, 2010). Rpn14 is a canonical WD40 protein and has a highly acidic surface area at the top face where the putative interacting surface of Rpt6 is located. In this paper, we describe the structure of a new crystal form of the yeast Rpn14 E384A mutant refined to 1.6 Å resolution in space group $P2_1$ with two molecules in the asymmetric unit. Overall, this structure is very similar to the previously characterized structure, including the

E384A site. However, a number of differences have been observed in loop regions.

2. Materials and methods

2.1. Cloning, expression, purification and crystallization

Saccharomyces cerevisiae Rpn14 with an E384A mutation (Kim *et al.*, 2010) was subcloned into pET28 vector (Novagen), which expresses N-terminally hexahistidine (His_6) tagged protein. Expression and purification of the recombinant protein was performed as described previously (Kim *et al.*, 2010). The purified protein was concentrated to 20 mg ml^{-1} by ultrafiltration in 25 m*M* Tris–HCl pH 7.5, 1 m*M* dithiothreitol. A monoclinic form of the Rpn14 E384A mutant was crystallized using 0.1 *M* sodium citrate pH 4.5, 0.2 *M* $MgCl_2$, 10%(*w*/*v*) PEG 3350 employing the hanging-drop vapour-diffusion method at 293 K. Crystals were soaked in cryoprotectant solution [10%(*v*/*v*) glycerol, 0.1 *M* sodium citrate pH 4.5, 0.2 *M* $MgCl_2$, 10%(*w*/*v*) PEG 3350].

2.2. X-ray data collection, structure determination and refinement

X-ray diffraction data sets were collected at 100 K on beamline BL44XU at SPring-8 (Hyogo, Japan). The data were processed using the *HKL*-2000 suite of programs (Otwinowski & Minor, 1997). The crystals belonged to space group $P2_1$, with two molecules in the asymmetric unit, corresponding to a Matthews coefficient of 1.94 Å^3 Da^{-1} (35.6% solvent content; Matthews, 1968). The data-collection statistics are summarized in Table 1. The crystal structure of the Rpn14 E384A mutant was solved by molecular replacement using *MOLREP* (Vagin & Teplyakov, 2010), with the structure of wild-type Rpn14 (PDB entry 3acp; Kim *et al.*, 2010) as the search model. The model was refined at 1.6 Å resolution using *REFMAC*5 (Murshudov *et al.*, 2011) and *Coot* (Emsley & Cowtan, 2004). Water

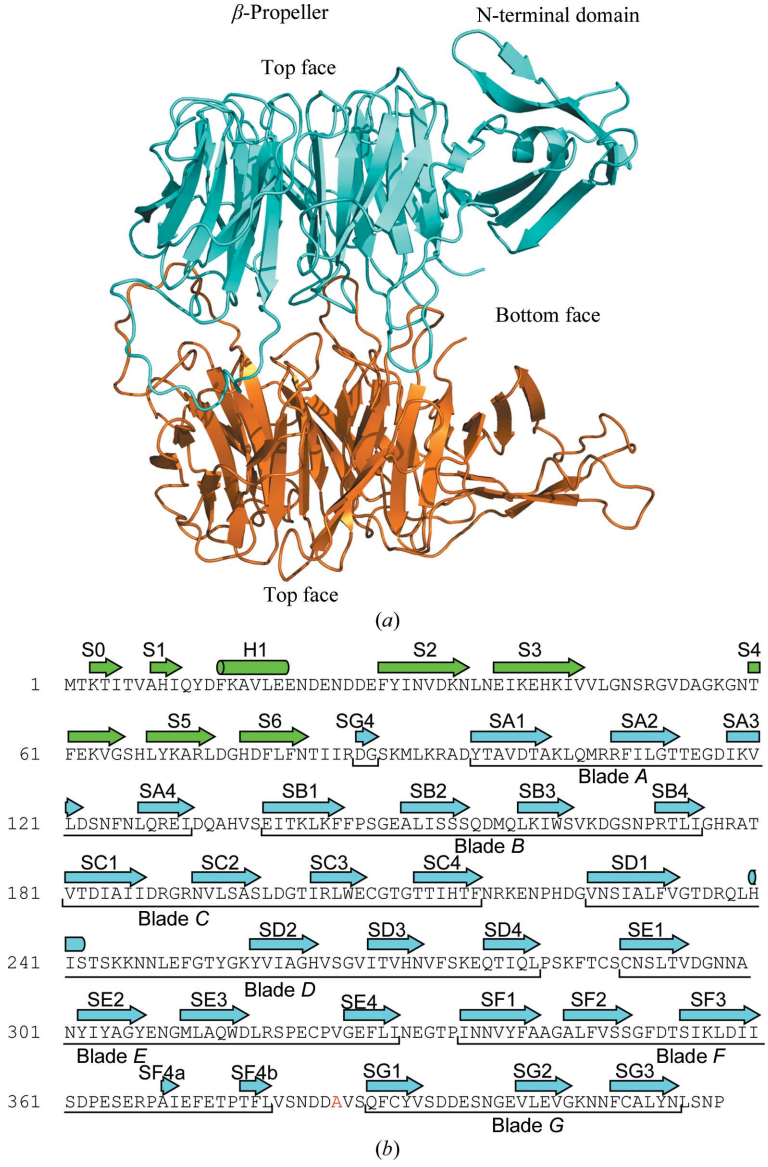

Figure 1
Structure of the yeast Rpn14 E384A mutant crystallized in space group $P2_1$. (*a*) Ribbon diagram of the two Rpn14 monomers in the asymmetric unit (chain *A*, cyan; chain *B*, orange). (*b*) Amino-acid sequence and secondary-structure elements of Rpn14. Secondary-structure elements are indicated above the sequence. The mutation-site residue (Glu384) is shown in red.

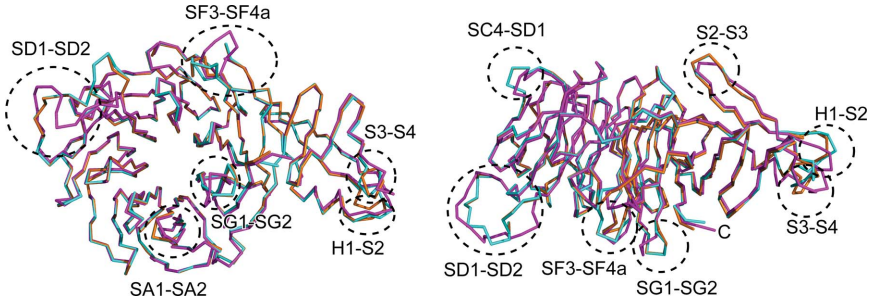

Figure 2
Comparison of the Rpn14 structures obtained from two different crystal forms. Molecules were superimposed using the C^{α} positions. Chains *A* and *B* of the Rpn14 E384A mutant crystallized in space group $P2_1$ are shown in cyan and orange, respectively; those in space group $P6_4$ (PDB entry 3acp; Kim *et al.*, 2010) are shown in magenta. Loops H1–S2, S2–S3, S3–S4, SC4–SD1, SD1–SD2, SF3–SF4a and SG1–SG2 of Rpn14 are circled with dotted lines.

Table 1
Data-collection and refinement statistics for the Rpn14 E384A mutant.

Values in parentheses are for the outer shell.

Data collection	
Space group	$P2_1$
Unit-cell parameters	
a (Å)	50.5
b (Å)	141.4
c (Å)	50.5
β (°)	95.7
Wavelength (Å)	0.9
Crystal-to-detector distance (mm)	175
Exposure time (s)	1
Resolution range (Å)	50.0–1.60 (1.62–1.60)
Total No. of reflections	349098
No. of unique reflections	90359
Completeness (%)	97.2 (97.2)
$R_{\rm merge}$† (%)	4.8 (52.8)
$\langle I/\sigma(I)\rangle$	19.5
Multiplicity	3.9 (3.7)
Refinement	
Resolution (Å)	24.47–1.60 (1.64–1.60)
No. of reflections	85676
$R_{\rm cryst}$ (%)	15.4 (22.3)
$R_{\rm free}$ (%)	23.5 (35.5)
R.m.s.d. bond lengths (Å)	0.008
R.m.s.d. bond angles (°)	1.1
No. of protein atoms	6750
No. of waters	417
Average *B* factors (Å^2)	
Protein	27.4
Solvent	49.4
Ramachandran plot (%)	
Most favoured region	87.1
Additional allowed region	12.2
Generously allowed region	0.7

† $R_{\rm merge} = \sum_{hkl}\sum_i |I_i(hkl) - \langle I(hkl)\rangle| / \sum_{hkl}\sum_i I_i(hkl)$.

molecules were built by *ARP/wARP* (Morris *et al.*, 2003). The Rpn14 E384A mutant structure was refined using anisotropic temperature factors. Model validation was carried out using *PROCHECK* from the *CCP*4 suite (Winn *et al.*, 2011). Structure figures were prepared using the *PyMOL* molecular-visualization system (DeLano, 2002).

Structure factors and coordinates have been deposited in the Protein Data Bank (PDB; http://www.rcsb.org/pdb) under accession code 3vl1.

3. Results and discussion

3.1. Structure of the Rpn14 E384A mutant in space group $P2_1$

We have previously determined the crystal structure of wild-type Rpn14, but the resolution of the structure was limited to 2.0 Å (Kim *et al.*, 2010). During the investigation, we noticed that an Rpn14 mutant with an Ala substitution of the Glu384 residue at the putative interacting surface for Rpt6 had a higher expression level in *E. coli* than the wild-type protein. This led us to undertake crystallization of the Rpn14 E384A mutant. The data-processing and refinement statistics are summarized in Table 1. The final refined model comprises residues 1–416 of both Rpn14 molecules (molecules *A* and *B*) in the asymmetric unit. Residues Gln11, Asp22, Asp25, Gln41, Arg93, Leu111, Thr114, Ser123, Ala133, Ser137, Lys161, Gln220, Thr254, Val267, Ile280, Lys285, Cys322, Gln387 and Glu395 in molecule *A*, and Tyr12, Val17, Lys34, Lys40, Leu111, Ser123, Asn124, Gln133, Glu149, Lys161, Ile175, Arg189, Arg203, Val267, Ser284, Lys285, Ser319, Glu321, Asn337, Val338, Ser348, Ile359, Ser386 and Ser392 in molecule *B* exhibit discrete conformations. Both molecules have a unique N-terminal domain and a C-terminal domain assuming a canonical seven-bladed β-propeller fold and they pack in a bottom-to-bottom manner related by a noncrystallographic twofold axis (Fig. 1). Although the overall structures of the two molecules are essentially the same, with the C^{α} atoms of molecules *A* and *B* having a root-mean-square (r.m.s.) deviation of 0.47 Å, three loops (H1–S2, S3–S4 and SF3–SF4a) and the C-terminal region exhibited different conformations (Fig. 2). Loops H1–S2 and S3–S4, which are located in

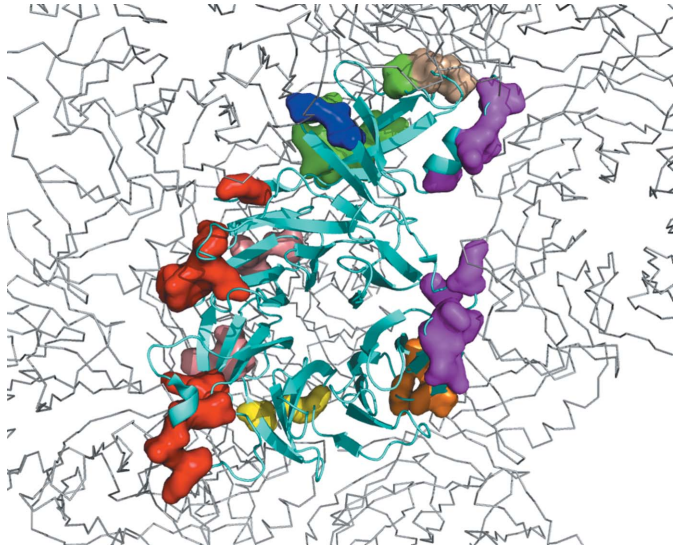

Figure 3
Overview of the crystal contacts. The crystal contacts of molecule *A* in the $P2_1$ crystal are shown in a spherical representation, in which each interface with the symmetry-related molecules is colour-coded ($x-1, y, z$, magenta; $-x, y+1/2, -z$, green; $x, y, z-1$, blue; $x, y, z+1$, orange; $x+1, y, z+1$, yellow; $-x+1, y+1/2, -z+1$, salmon; $x+1, y, z$, red).

the N-terminal domain, loop SF3–SF4a and the C-terminal region are on the bottom face of the β-propeller. Molecules *A* and *B* interact through an extensive interface, burying a total of 4380 Å^2 of surface area (2190 Å^2 each for molecules *A* and *B*). The interface involves 11 loops (SA1–SA2, SA3–SA4, SB1–SB2, SB3–SB4, SC1–SC2, SC3–SC4, SD1–SD2, SE1–SE2, SF1–SF2, SF3–SF4a and SG1–SG2) and the C-terminal region.

Crystal contacts are present between the asymmetric unit and ten symmetry-related molecules ($x + 1, y, z$; $x - 1, y, z$; $x, y, z + 1$; $x, y, z - 1$; $x + 1, y, z + 1$; $x - 1, y, z - 1$; $-x, y + 1/2, -z$; $-x + 1, y + 1/2, -z + 1$; $-x, y - 1/2, -z$; $-x + 1, y - 1/2, -z + 1$; Table 2). The interface with molecules in crystal contact has an area of 5430 Å for molecule *A* and 5760 Å for molecule *B* (Fig. 3). The interfaces involve 18 loops and eight sheets (loops N–S1, S1–H1, H1–S2, S2–S3, S3–S4, S5–S6, SG4–SA1, SA2–SA3, SA3–SA4, SA4–SB1, SB4–SC1, SC4–SD1, SD1–SD2, SD4–SE1, SE2–SE3, SE3–SE4, SF3–SF4a and SG2–SG3; sheets S3, S5, SA3, SA4, SC4, SD3, SE2 and SE3).

3.2. Structural comparison with wild-type Rpn14

Although the overall structure of the mutant Rpn14 is almost identical to that of the wild type (the r.m.s. deviations for C$^\alpha$ atoms are 1.8 Å for molecule *A* and 1.9 Å for molecule *B*), there are several differences (Figs. 2 and 4). The N-terminal region (residues 3–5) forms an S0 strand and three loops (H1–S2, S2–S3 and S3–S4) in the N-terminal domain and five loops (SA1–SA2, SC4–SD1, SD1–SD2, SF3–SF4a and SG1–SG2) in the C-terminal β-propeller exhibit different conformations. Only loop SC4–SD1 is located on the top face of the β-propeller. Loop SC4–SD1 and the N-terminal domain are situated at opposite ends of Rpn14. The conformation of this loop is not conserved and it is located far from the putative binding site in the negatively charged area on the top face. This conformation does not affect the binding of Rpt6. The remaining C-terminal β-propeller loops, SA1–SA2, SD1–SD2, SF3–SF4a and SG1–SG2, contribute to the interaction between molecules *A* and *B*. The loop SD1–SD2 is shifted significantly compared with that in wild-type Rpn14. Part of the SD1–SD2 loop (residues 240–242) is replaced by a 3_{10}-helix structure. The surface area occupied by loop SD1–SD2 is 751 Å^2, corresponding to 34.3% of the total interface area. In the N-terminal domain of the mutant Rpn14, loops H1–S2, S2–S3 and S3–S4 are involved in crystal contact interactions.

In the wild-type structure (space group $P6_4$), there are crystal contacts with six symmetry-related molecules ($-x + 1, -y, z$; $x - y, x - 1, z - 1/3$; $y + 1, -x + y + 1, z + 1/3$; $-y + 1, x - y - 1, z + 1/3$; $-x + y + 2, -x + 1, z - 1/3$; $-x + 2, -y + 1, z$). The interface with molecules in crystal contact has an area of 4560 Å. The interfaces involve 14 loops and eight sheets (loops S3–S4, S5–S6, SG4–SA1, SB3–SB4, SC4–SD1, SD1–SD2, SD3–SD4, SD4–SE1, SE1–SE2, SF2–SF3, SF3–SF4a, SF4b–SG1, SG2–SG3 and SG–Ct; sheets S3, S6, SB4, SC3, SD2, SD3, SD4 and SF3)

The two crystal forms have different crystal contact sites. In the Rpn14 E384A mutant crystal loops and sheets in the N-terminal domain (N–S1, H1–S2, S1–H1 and S2–S3), blade *A* (SA2–SA3, SA3, SA3–SA4, SA4 and SA4–SB1) and blade *E* (SE2, SE2–SE3, SE3 and SE3–SE4) are involved in crystal contacts, whereas in the wild-type Rpn14 crystal loops and sheets in blade *B* (SB3–SB4 and SB4), blade *D* (SD2, SD3–SD4, SD3–SD4 and SD4) and blade *F* (SE2, SE2–SE3, SE3 and SE3–SE4) are involved in crystal contacts.

Glu384 is positioned in the centre of the surface acidic cluster that is not critical for interaction with Rpt6 (Kim *et al.*, 2010). Although the overall conformation of these clusters is very similar to that in the wild-type protein, the side chain of Lys405 has a different conformation, displaying a visible change in the surface-charge distribution

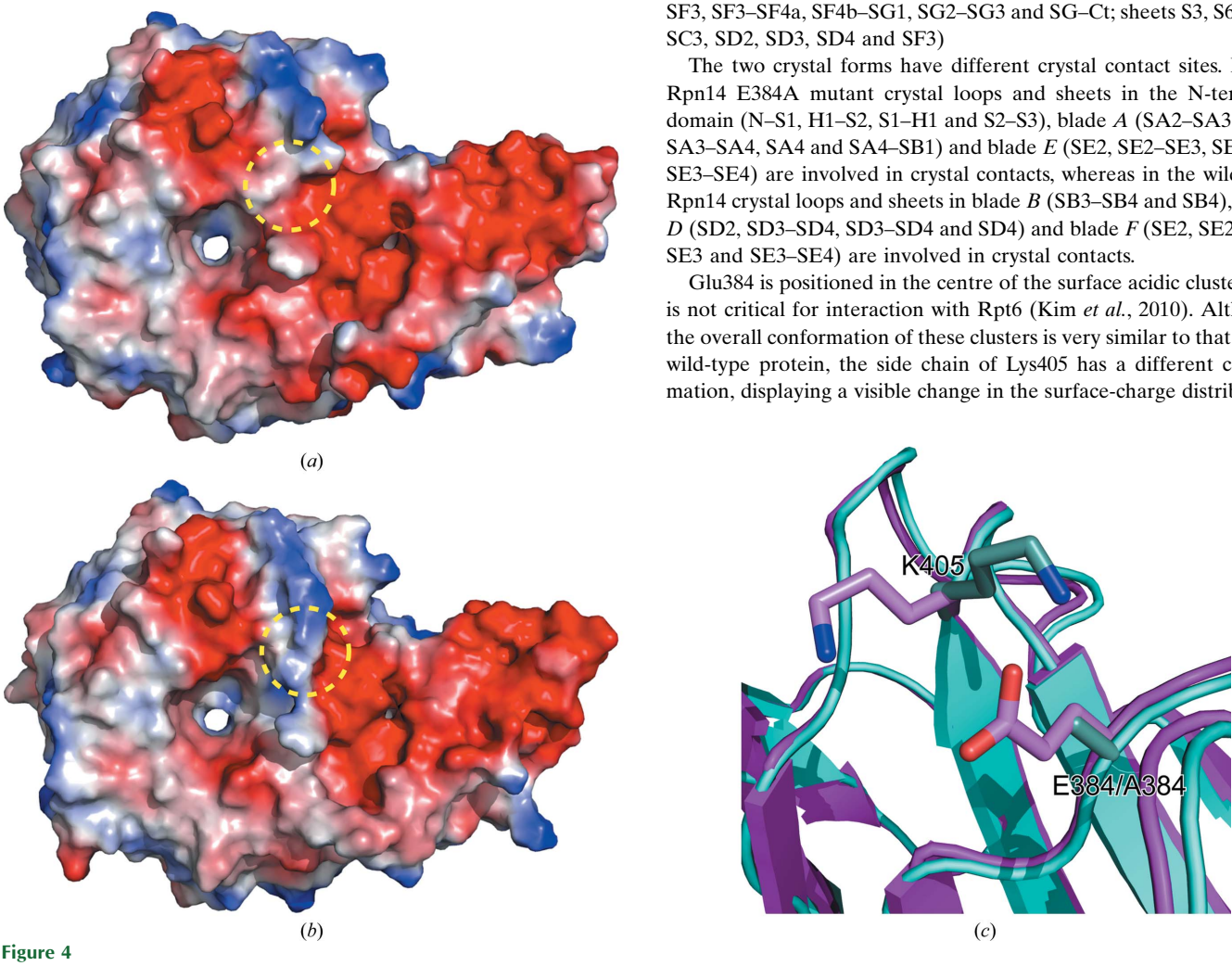

(*a*) (*b*) (*c*)

Figure 4
Comparison of the mutation site in wild-type Rpn14 and the Rpn14 E384A mutant. Surface-potential representations are shown for wild-type Rpn14 (*a*) and the Rpn14 E384A mutant (*b*). The mutation site is shown in a circle. Red, blue and white represent acidic, basic and neutral, respectively. (*c*) Close-up view of the mutation site in Rpn14. Wild-type Rpn14 is shown in cyan and the Rpn14 E384A mutant is shown in magenta. The side chains of residues 384 and 405 are shown as stick models.

Table 2
Hydrogen bonds between symmetry-related molecules in the crystals.

The letters in columns *X* and *Y* of the table indicate the names of the blades in the WD40 propeller domains. Each blade includes four sheets and four loops. The C-terminal loop in each blade, *e.g.* SA4–SB1, was included in the preceding blade. Nt, N-terminal domain.

$P2_1$, molecule *A*			$P2_1$, molecule *B*			$P6_4$		
X	*Y*	Symmetry operation	*X*	*Y*	Symmetry operation	*X*	*Y*	Symmetry operation
Nt	Nt	$x + 1, y, z$	Nt	Nt	$x, y, z + 1$	*B*	*D*	$-x + 1, -y, z$
D	*A*, *G*	$x + 1, y, z$	*D*	*A*, *G*	$x, y, z + 1$	*C*	*D*	$-x + 1, -y, z$
E	Nt	$x + 1, y, z$	*E*	Nt	$x, y, z + 1$	*D*	*B*, *C*	$-x + 1, -y, z$
F	Nt	$x + 1, y, z$	*F*	Nt	$x, y, z + 1$	*G*	*F*, *G*	$-x + 2, -y + 1, z$
Nt	Nt, *E*, *F*	$x - 1, y, z$	Nt	Nt, *E*, *F*	$x, y, z - 1$	*F*	*G*	$-x + 2, -y + 1, z$
A	*D*	$x - 1, y, z$	*A*	*D*	$x, y, z - 1$	Nt	*D*, *E*	$-x + y + 2, -x + 1, z - 1/3$
G	*D*	$x - 1, y, z$	*G*	*D*	$x, y, z - 1$	*F*	*C*	$x - y, x - 1, z - 1/3$
A	Nt	$x, y, z + 1$	*A*	Nt	$x + 1, y, z$	*G*	*D*	$x - y, x - 1, z - 1/3$
Nt	*A*	$x, y, z - 1$	Nt	*A*	$x - 1, y, z$	*C*	*F*	$y + 1, -x + y + 1, z + 1/3$
B	Nt	$x + 1, y, z + 1$	*B*	Nt	$x + 1, y, z + 1$	*D*	*G*	$y + 1, -x + y + 1, z + 1/3$
C	Nt	$x + 1, y, z + 1$	*C*	Nt	$x + 1, y, z + 1$	*D*	Nt	$-y + 1, x - y - 1, z + 1/3$
Nt	*B*, *C*	$x - 1, y, z - 1$	Nt	*B*, *C*	$x - 1, y, z - 1$	*E*	Nt	$-y + 1, x - y - 1, z + 1/3$
Nt	Nt	$-x, y + 1/2, -z$ (*B*)	Nt	Nt	$-x, y - 1/2, -z$ (*A*)			
D	*D*, *E*	$-x + 1, y + 1/2, -z + 1$ (*B*)	*D*	*D*, *E*	$-x + 1, y - 1/2, -z + 1$ (*A*)			
E	*D*, *E*	$-x + 1, y + 1/2, -z + 1$ (*B*)	*E*	*D*, *E*	$-x + 1, y - 1/2, -z + 1$ (*A*)			

(Fig. 4). However, *in vitro* binding studies suggest that this conformational change is not essential for the binding of Rpt6 (Kim *et al.*, 2010). It is likely that the acidic surface of Glu384 does not contribute to the interaction with Rpt6.

4. Conclusion

We report a new crystal form of the Rpn14 E384A mutant at 1.6 Å resolution in space group $P2_1$. Although its overall structure is very similar to the structure described for the wild-type protein, minor differences in loop regions and mutation sites were observed. Some of the bottom-face loops exhibited conformational flexibility, and a change in the surface-charge distribution was also observed. The improved high-resolution structure of Rpn14 presented here provides a useful framework for the understanding of proteasome-assembly mechanisms.

This work was supported in part by grants from the Ministry of Education, Culture, Sports, Science and Technology (MEXT) of Japan: a Grant-in-Aid for Scientific Research on Innovative Areas (TM), a Grant-in-Aid for Challenging Exploratory Research (TM), The Naito Foundation (TM), a Grant-in-Aid for Specially Promoted Research (KT), a Grant-in-Aid for Young Scientists (YS) and the Targeted Proteins Research Program (KK, KT and TM). Diffraction data were collected at Osaka University using beamline BL44XU at SPring-8 equipped with an MX225-HE detector (Rayonix), financially supported by Academia Sinica and National Synchrotron Radiation Research Center (Taiwan).

References

DeLano, W. (2002). *PyMOL*. http://www.pymol.org.
Emsley, P. & Cowtan, K. (2004). *Acta Cryst.* D**60**, 2126–2132.
Finley, D. (2009). *Annu. Rev. Biochem.* **78**, 477–513.
Funakoshi, M., Tomko, R. J., Kobayashi, H. & Hochstrasser, M. (2009). *Cell*, **137**, 887–899.
Kaneko, T., Hamazaki, J., Iemura, S., Sasaki, K., Furuyama, K., Natsume, T., Tanaka, K. & Murata, S. (2009). *Cell*, **137**, 914–925.
Kim, S., Saeki, Y., Fukunaga, K., Suzuki, A., Takagi, K., Yamane, T., Tanaka, K., Mizushima, T. & Kato, K. (2010). *J. Biol. Chem.* **285**, 15159–15166.
Le Tallec, B., Barrault, M. B., Guérois, R., Carré, T. & Peyroche, A. (2009). *Mol. Cell*, **33**, 389–399.
Matthews, P. C. (1968). *Int. J. Soc. Psychiatry*, **14**, 125–133.
Morris, R. J., Perrakis, A. & Lamzin, V. S. (2003). *Methods Enzymol.* **374**, 229–244.
Murata, S., Yashiroda, H. & Tanaka, K. (2009). *Nature Rev. Mol. Cell Biol.* **10**, 104–115.
Murshudov, G. N., Skubák, P., Lebedev, A. A., Pannu, N. S., Steiner, R. A., Nicholls, R. A., Winn, M. D., Long, F. & Vagin, A. A. (2011). *Acta Cryst.* D**67**, 355–367.
Otwinowski, Z. & Minor, W. (1997). *Methods Enzymol.* **276**, 307–326.
Ramos, P. C. & Dohmen, R. J. (2008). *Structure*, **16**, 1296–1304.
Roelofs, J., Park, S., Haas, W., Tian, G., McAllister, F. E., Huo, Y., Lee, B.-H., Zhang, F., Shi, Y., Gygi, S. P. & Finley, D. (2009). *Nature (London)*, **459**, 861–865.
Rosenzweig, R. & Glickman, M. H. (2008). *Biochem. Soc. Trans.* **36**, 807–812.
Saeki, Y., Toh-E, A., Kudo, T., Kawamura, H. & Tanaka, K. (2009). *Cell*, **137**, 900–913.
Sakata, E., Stengel, F., Fukunaga, K., Zhou, M., Saeki, Y., Förster, F., Baumeister, W., Tanaka, K. & Robinson, C. V. (2011). *Mol. Cell*, **42**, 637–649.
Tanaka, K. (2009). *Proc. Jpn Acad. Ser. B Phys. Biol. Sci.* **85**, 12–36.
Tomko, R. J., Funakoshi, M., Schneider, K., Wang, J. & Hochstrasser, M. (2010). *Mol. Cell*, **38**, 393–403.
Vagin, A. & Teplyakov, A. (2010). *Acta Cryst.* D**66**, 22–25.
Winn, M. D. *et al.* (2011). *Acta Cryst.* D**67**, 235–242.